



Oblique-incidence reflectivity difference application for morphology detection

HONGLEI ZHAN,^{1,2,3,*} KUN ZHAO,^{1,2} HUIBIN LÜ,⁴ KUIJUAN JIN,⁴ GUOZHEN YANG,⁴ AND XIAOHONG CHEN¹

¹State Key Laboratory of Petroleum Resources and Prospecting, China University of Petroleum, Beijing 102249, China

²Beijing Key Laboratory of Optical Detection Technology for Oil and Gas, China University of Petroleum, Beijing 102249, China

³Department of Material Science and Engineering, China University of Petroleum, Beijing 102249, China

⁴Institute of Physics, Chinese Academy of Sciences, Beijing 100190, China

*Corresponding author: zhanhl@cup.edu.cn

Received 10 August 2017; revised 1 September 2017; accepted 19 September 2017; posted 20 September 2017 (Doc. ID 304637); published 12 October 2017

Analogous with scanning electron microscopy, we use an oblique-incidence reflectivity difference (OIRD) approach for morphology detection. By scanning the active carbon clusters in a one-dimensional way and the reservoir rocks in a two-dimensional way, the morphology of the samples' surface can be revealed in OIRD signal images. High OIRD signals of active carbon samples refer to the centralized distribution areas of carbon, and the fluctuations are caused by the uneven distribution of carbon pellets. OIRD intensity is proportional to the thickness of materials. In terms of rocks, the trough areas with smaller values refer to the low-lying fields. The areas with relatively large OIRD intensities correspond to the protuberance areas of rocks. Consequently, OIRD is a sensitive yet rapid measure of surface detection in material and petrogeology science. © 2017 Optical Society of America

OCIS codes: (110.0110) Imaging systems; (120.4820) Optical systems; (350.4600) Optical engineering.

<https://doi.org/10.1364/AO.56.008348>

1. INTRODUCTION

Measuring the surface dielectric properties of materials directly involves a number of theoretical and technical challenges, including realizing nondestructive detection, understanding the signal information of the sample, and measuring the sample under the common condition. An optical microscope is a common optical instrument to recognize the magnification imaging that cannot be distinguished with eyes. Scanning electron microscopy (SEM) and atomic force microscopy (AFM) are appropriate ways to describe the surface structures and morphology information [1]. However, some materials cannot be measured by SEM, because a vacuum environment is necessary when measuring, and liquid water is not allowed because it may volatilize and harm the SEM setup. Although AFM has a very large resolution of atoms, its scanning velocity is very small and time length is very long.

In recent years, various optical techniques have emerged as important tools for detecting the morphology of materials and rocks [2,3]. Representative and newly developed techniques include terahertz (THz) spectroscopy and oblique-incidence reflectivity difference (OIRD) [4–7]. A THz wave can be applied to rocks mapping the mineralogy and used to obtain high-spatial resolution maps of the spatially varying dielectric permittivity of heterogeneous materials [8,9]. The anisotropy in

THz parameters of the oil shale can be extracted and employed to characterize the oil yield precisely [10]. The THz spectrum and its imaging are gradually and successfully employed in the petroleum field [11–14]. Meanwhile, THz chemical imaging is appropriate to reveal hydrogen bond distributions [15]. Consequently, they both can measure the physical information of materials, but relative to THz spectroscopy, OIRD has a larger spatial resolution, which is of significance for some substances such as reservoir rocks.

OIRD measures the difference in reflectivity between *s*- and *p*-polarized lights; thus, it is very sensitive to the dielectric and surface properties of the material surface. An OIRD image can reveal the hybridization and determine the thickness of oligonucleotides in the microarray, simultaneously. According to previous reports, OIRD has a time resolution of 20 μs, a spatial resolution of 0.4 nm, and a detection sensitivity of 14 fg of protein per spot [16–18]. OIRD signal intensities are related to the physical properties of materials. According to the classical three-layer model,

$$\Delta_p - \Delta_s = \frac{(-i)4\pi d \sqrt{\epsilon_0} \epsilon_s \cos \varphi_{\text{inc}} \sin^2 \varphi_{\text{inc}}}{\lambda(\epsilon_s - \epsilon_0)(\epsilon_s \cos^2 \varphi_{\text{inc}} - \epsilon_0 \sin^2 \varphi_{\text{inc}})} \times \frac{(\epsilon_d - \epsilon_0)(\epsilon_d - \epsilon_s)}{\epsilon_d},$$

where ε_0 , ε_s , φ_{inc} , and λ represent the relative permittivity of the environment, relative permittivity of the basement, incidence angle, and wavelength, the OIRD signal intensity is a function of dielectric constant ε_d and effective thickness d . For the real-time detection of morphology, d would change as the scanning position is moving. In the OIRD system, a two-dimensional motorized stage is used to fix a sample and obtain the OIRD signals of samples. The stage can be motioned in a two-dimensional range to obtain images and in a one-dimensional range to obtain a line information.

Recently, more promising applications were reported for the label-free, high throughput detection of interactions of biological molecules [19]. The OIRD technique can not only characterize the defects but also detect the adsorption dynamics of liquid molecules [20]. The layered distribution of the dielectric properties in shales and the uniform distribution in sandstones can be clearly identified using OIRD signals. The dielectric and surface properties are closely related to the hydrocarbon-bearing features in oil gas reservoirs so that the precise measurement carried with OIRD can help improve the recovery efficiency [21]. In this research, OIRD was used to detect the morphology information with one-dimensional and two-dimensional scanning. Active carbon and reservoir rocks were measured and their OIRD images were validated by SEM analysis. The work allows us to achieve more approaches for the detection of morphology information in materials science and the petrogeology industry.

2. EXPERIMENTAL METHODS

As depicted in Fig. 1, we show the scheme of the OIRD system for the label-free and real-time detection of reservoir rocks. A p -polarized He-Ne laser with a wavelength of $\lambda = 632.8$ nm is selected as the detection light beam. The laser passes through a polarizer (P) to ensure p -polarized incidence. The light beam then passes through a photoelastic modulator (PEM) so that the polarization of the light beam oscillates from p - to s -polarization at the frequency of 50 kHz. The laser beam output from the PEM enters a phase shifter that would introduce a variable phase difference Φ_{ps} between the p - and s -polarization components. The light beam is focused by an optical lens into the sample surface near the Brewster angle $\theta = 57.6^\circ$. The reflected beam passes through a second lens and enters a polarization analyzer (PA) with the transmission axis from s -polarization. At last the intensity of the reflected beam is

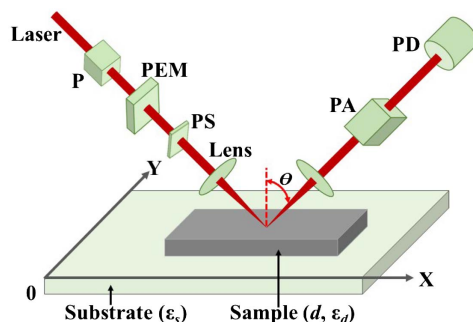


Fig. 1. Sketch of OIRD system for the morphology detection of the active carbon and reservoir rocks.

detected by a silicon photodiode (PD). Two lock-in amplifiers are employed to measure the first harmonic $I(1\Omega)$ and the second harmonic $I(2\Omega)$ signals. Before the scanning measurement, we adjust the phase shifter and polarization analyzer so that the $I(2\Omega)$ and $I(1\Omega)$ signals are equal to zero to improve the sensitivity of the measurement [22,23].

In the experiment, an active carbon and two different rocks were used for one-dimensional and two-dimensional morphology information. Generally, there are no special requirements on sample preparation for OIRD detection. The active carbon pellets adhered tightly onto the fiber cloth to form the active carbon fiber cloth (ACFC), which was taken from the active carbon breathing mask. The rocks were cored at a depth of ~ 3000 m in the horizontal direction from different oil fields. The rocks were cut and then polished to confirm the parallelism between the upper and lower surfaces of the cores before OIRD measurement. After the samples were prepared, the active carbon or reservoir rocks were fixed on the two-dimensional stage. The scanning range was a $1\text{ mm} \times 1\text{ mm}$ rectangle area. The scanning step length was set as $4\ \mu\text{m}$. The measurements were performed under ambient conditions. Finally, we detected the real part $\text{Re}\{\Delta_p - \Delta_s\}$ and the imaginary part $\text{Im}\{\Delta_p - \Delta_s\}$ signal of the samples. In this research, $\text{Im}\{\Delta_p - \Delta_s\}$ was used as the parameter to detect the morphology.

3. RESULTS AND DISCUSSION

A basic investigation was initially performed about the OIRD reflectivity response of ACFC by two-dimensional scanning. Figure 2(a) is the intensity profile taken along a line in the active carbon sample. $\text{Im}\{\Delta_p - \Delta_s\}$ alters with the change of scanning distance. Several maximum signals can be observed and respective peak wave are located at different positions; meanwhile, fluctuations are also observed in some special areas, indicating that the morphology information of the sample surfaces are reflected in the OIRD signals. To determine the structural information of the ACFC sample surfaces, SEM was then employed to analyze active carbon investigated with OIRD. Secondary electron (SE) was used to obtain a new set of images shown in Fig. 2(b). SE was very sensitive to the surface morphology, thus making it an effective method for observing the surface morphology. According to Fig. 2(b), the carbon reflected a centralized distribution in some areas other than distributed evenly. Besides, the enlarged image shows that the pellets were also uneven in the active carbon areas. Active carbon was a kind of porous material whose void radius approximately varied from ~ 100 nm to $\sim 50\ \mu\text{m}$. Comparing the OIRD signals and the SEM images, it can be revealed that the areas with high OIRD signals refer to the centralized distribution areas of active carbon, and the fluctuations of OIRD signals are caused by the uneven distribution carbon pellets. In terms of the areas with smaller OIRD signal intensities, the ACFC sample has little carbon pellets. The fiber cloth wires are criss-crossed between the areas of carbon pellets. The OIRD signal is related to the distribution of active carbons, which can be revealed by the comparison of OIRD response and SEM images. Consequently, OIRD measurement characterized

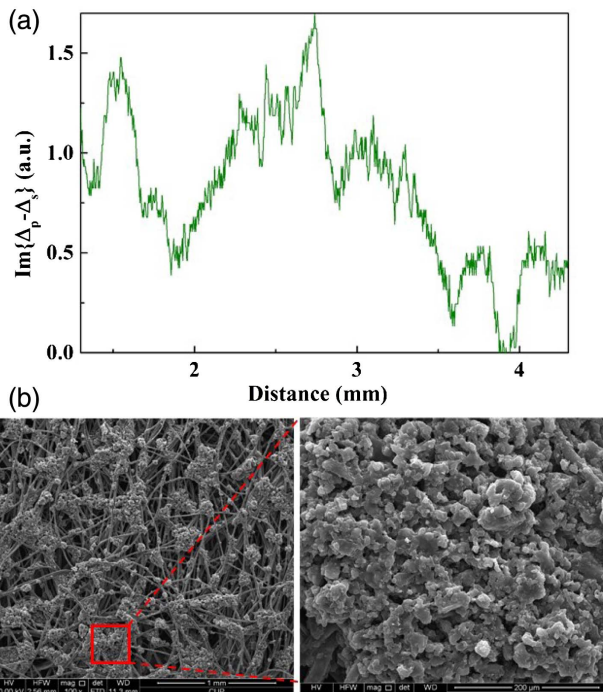


Fig. 2. Morphology analysis of active carbon samples. (a) Distance dependent $\text{Im}\{\Delta_p - \Delta_s\}$ intensities of active carbon sample. (b) SEM images of ACFC: the right picture refers to the enlarged image of the left one.

the surface morphology of ACFC samples with one-dimensional scanning.

To further explore the practicality of the OIRD approach being applied in morphology detection of the petroleum reservoir, we selected two pieces of rocks 3 km underground and performed the OIRD measurement. An optical microscope analysis was initially performed before the rocks were measured by OIRD. Figure 3 shows a set of optical microscope images of the mentioned two reservoir rocks. The spatial resolution in horizontal and vertical directions were about $200\ \mu\text{m}$. The gray level distribution mainly reflects the particle distribution that

was caused by the rocks' components. Consequently, optical microscope images indicate that the morphology of rocks were irregularly polygon and dispersed well.

Figure 4 shows three-dimensional OIRD signal mapping of two reservoir rocks cored at a depth of $\sim 3000\ \text{m}$ in the horizontal direction. The square of each image is $300\ \mu\text{m} \times 300\ \mu\text{m}$, and the $\text{Im}\{\Delta_p - \Delta_s\}$ values reflect the relative variance. The signal intensities exhibited several peaks and troughs on the surfaces in imaginary images, showing the position-dependent uniformity of the physical properties. It is apparent that the trough areas with different sizes are randomly distributed throughout the surface of reservoir rocks. Large granules can have a width range from $\sim 20\ \mu\text{m}$ to $\sim 130\ \mu\text{m}$ shown in Fig. 4(a). In the three-dimensional systems of the imaginary parts, the trough areas appear to be approximately, but not absolutely, equal to each other. In contrast to Fig. 4(a), Fig. 4(b) plots a lot of trough areas with different sizes smaller than $100\ \mu\text{m}$. Similarly, the areas are randomly distributed throughout the surfaces and are nondirectional relative to being over the whole areas. Compared to Fig. 3 obtained with an optical microscope, Fig. 4 shows the more obvious contrast at different points. Meanwhile, OIRD signal images reflect the dielectric properties' distribution, which can help reveal more information of physical properties in the concentrated areas of high or low intensities. The signals continuously changed at near positions. According to the OIRD images, it is revealed that OIRD images of rock surfaces contributed variously at different positions, indicating that OIRD signals are related to the physical properties of materials.

The approximately irregular structures and the uneven morphology features of rocks are clearly reflected in Fig. 4. The type relates to the orientation of rock particles or a crevice. To detect the real structural information of the rock surfaces, SEM was then employed to analyze the rocks measured by OIRD. SE modes were used to obtain the morphology images of relative reservoir rocks. Figure 5 shows the SEM images of two rocks: (a) shows the SE morphology image of a reservoir rock with a scale line of $200\ \mu\text{m}$; (b) shows the SE morphology image of another reservoir rock with a scale line of $100\ \mu\text{m}$. The SE images revealed the microdefects such as cracks and orientations

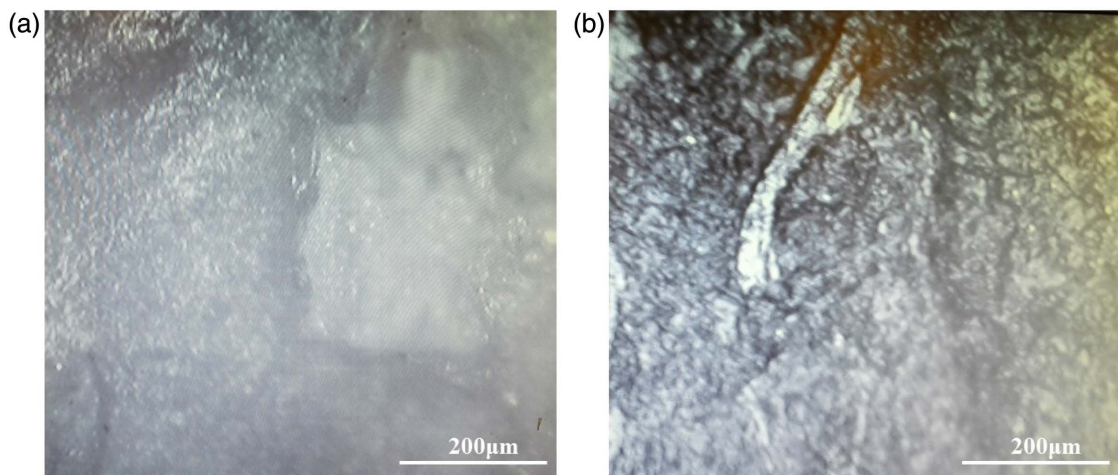


Fig. 3. Optical microscope analysis of the surfaces of reservoir rocks.

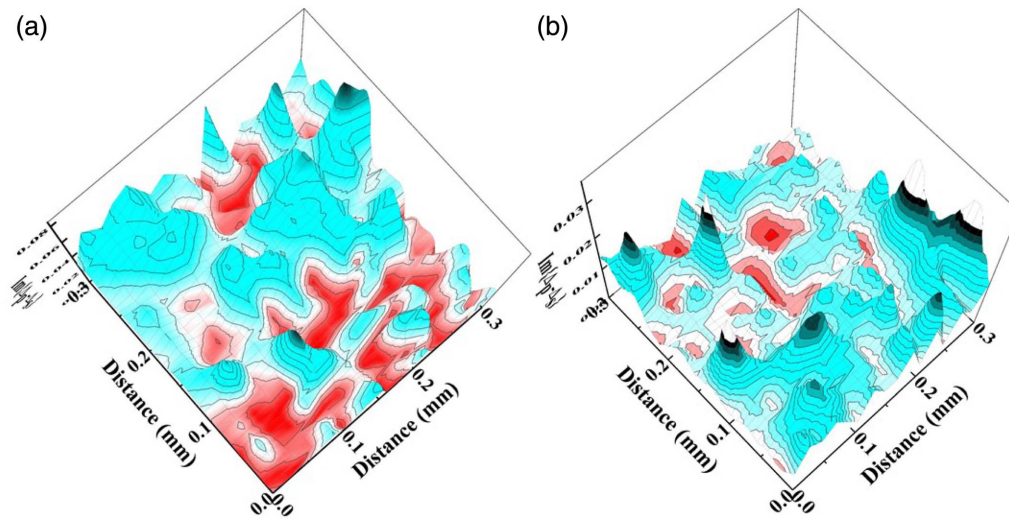


Fig. 4. OIRD images of two reservoir rocks in which random regions were scanned by the OIRD system. Red and cyan represent small and large OIRD signal intensities, respectively.

of rock particles in the rocks, as clearly shown in the OIRD images with the corresponding imaginary signals. In Fig. 5(a), some differently sized particles were observed with clear annular cracks between them. These annular cracks surround some low-lying areas. In Fig. 5(b), the rock is denser, and the defects have relatively smaller size.

According to comparison between Figs. 4 and 5, high similarity can be observed in terms of the structures in two reservoir rocks. OIRD signal intensity is a function of effective thickness d and dielectric constant ϵ_d on the basis of the widely used formula in the experimental section. OIRD intensity is proportional to the thickness of materials. Consequently, the trough areas (red areas) with smaller values in Fig. 4 refer to the low-lying fields. They possess similar-size ranges and contour shapes in both reservoir rocks. In terms of cyan areas, which have relatively large OIRD intensities, they correspond to the protuberances areas in Fig. 5. The differences of OIRD intensities in these areas may be caused by the dielectric

constant variances. The elemental components with different atomic masses are uniformly distributed through the cyan areas. Therefore, the OIRD technique is a very promising and practical technology to detect the morphology information and is a convenient supplementary method that can be combined with conventional methods.

Similar to some other technologies, there are some limitations of the new technique. For instance, the baseline of the signal should be regulated in each measurement. Besides, more mathematical methods should be developed to analyze the data of the signal. Overall, this study focuses on applying the OIRD approach to active carbon and reservoir rocks, and proves that the OIRD is a very practical technique for detecting morphology. The morphology features can be clearly observed in the images of $\text{Im}\{\Delta_p - \Delta_s\}$ by both one-dimensional and two-dimensional scanning. The detection results in the OIRD images are in agreement with those of the SEM mappings. Accordingly, the research suggests that this approach used to

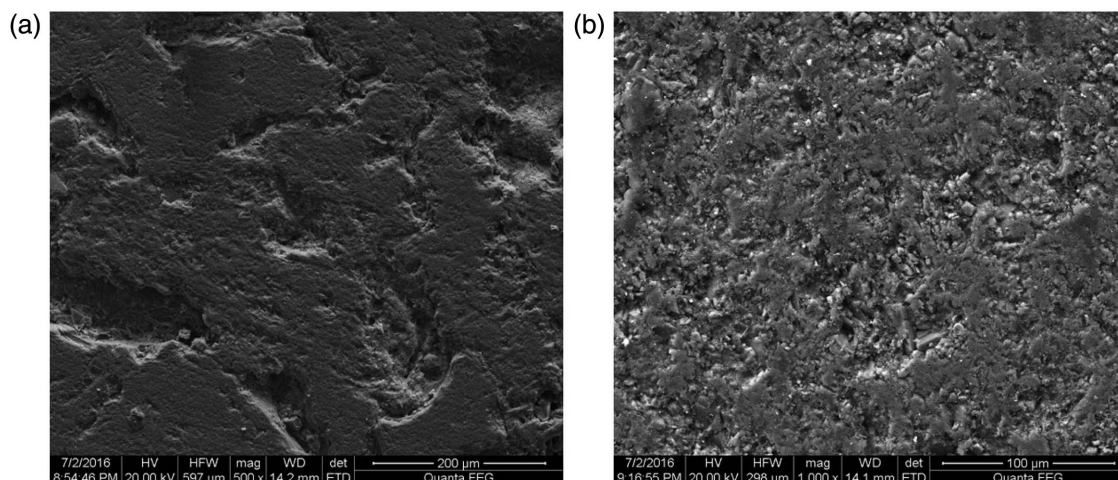


Fig. 5. SEM images of reservoir rocks that were measured by OIRD.

characterize the morphology of the reservoir rock should combine previous techniques, such as optical microscopy, the SEM technique, and newly developed optical methods, such as terahertz (THz) spectroscopy [3,8,9]. Compared to the THz technique, OIRD has a higher spatial resolution due to the light source possessing a shorter wavelength. Relative to microscope and SEM techniques, OIRD can detect the dielectric properties of the materials that are useful in revealing the physical or chemical information. As reported in previous articles, the OIRD signal, which reflects the differences between the reflectivity of *s*- and *p*-polarized light, is related to the material's dielectric and surface properties so that it is a sensitive surface detection technique [21,24]. OIRD is a very promising and practical technology for detecting the morphology of general materials and reservoir rocks.

4. CONCLUSION

In summary, by using a newly developed OIRD technique, we were able to detect the morphology features of samples with both one-dimensional and two-dimensional scanning. This optical approach has extremely high sensitivity to the distribution of structural and componential properties. We tested this technique on active carbons and reservoir rocks, and compared the OIRD results to SEM mappings, indicating that the OIRD analysis can be clearly validated. The technique is fast (limited only by the speed of the mechanical scanning) and is easily applied to any space due to the simple system composition. It can be expected that the OIRD technique is a convenient supplementary morphology detection technique for conventional methods.

Funding. National Natural Science Foundation of China (NSFC) (11574401); National Basic Research Program of China (2014CB744302); Science Foundation of China University of Petroleum-Beijing (2462017YJRC029); China Petroleum and Chemical Industry Association Science and Technology Guidance Program (2016-01-07).

REFERENCES

1. M. Sujka and J. Jamroz, " α -Amylolytic activity of native potato and corn starches—SEM, AFM, nitrogen and iodine sorption investigations," *LWT Food Sci. Technol.* **42**, 1219–1224 (2009).
2. M. A. Tianshou and P. Chen, "Study of meso-damage characteristics of shale hydration based on CT scanning technology," *Pet. Explor. Dev.* **41**, 249–256 (2014).
3. N. S. Greeney and J. A. Scales, "Non-contacting characterization of the electrical and mechanical properties of rocks at submillimeter scales," *Appl. Phys. Lett.* **100**, 124105 (2012).
4. H. L. Zhan, Q. Li, K. Zhao, L. W. Zhang, Z. W. Zhang, C. L. Zhang, and L. Z. Xiao, "Evaluating PM_{2.5} at a construction site using terahertz radiation," *IEEE Trans. Terahertz Sci. Technol.* **5**, 1028–1034 (2015).
5. A. Kar, A. Saha, and N. Goswami, "Long-range surface plasmon-induced tunable ultralow threshold optical bistability using graphene sheets at terahertz frequency," *Appl. Opt.* **56**, 2321–2329 (2017).
6. H. Nasari and M. S. Abrishamian, "Terahertz bistability and multistability in graphene/dielectric Fibonacci multilayer," *Appl. Opt.* **56**, 5313–5322 (2017).
7. J. P. Landry, J. Gray, M. K. Toole, and X. D. Zhu, "Incidence-angle dependence of optical reflectivity difference from an ultrathin film on a solid surface," *Opt. Lett.* **31**, 531–533 (2006).
8. N. S. Greeney and J. A. Scales, "Dielectric microscopy with submillimeter resolution," *Appl. Phys. Lett.* **91**, 222909 (2007).
9. J. A. Scales and M. Batzle, "Millimeter wave spectroscopy of rocks and fluids," *Appl. Phys. Lett.* **88**, 062906 (2006).
10. X. Y. Miao, H. L. Zhan, K. Zhao, Y. Z. Li, Q. Sun, and R. M. Bao, "Oil yield characterization by anisotropy in optical parameters of the oil shale," *Energy Fuels* **30**, 10365–10370 (2016).
11. H. L. Zhan, K. Zhao, and L. Z. Xiao, "Spectral characterization of the key parameters and elements in coal using terahertz spectroscopy," *Energy* **93**, 1140–1145 (2015).
12. H. L. Zhan, S. X. Wu, R. M. Bao, L. N. Ge, and K. Zhao, "Qualitative identification of crude oils from different oil fields using terahertz time-domain spectroscopy," *Fuel* **143**, 189–193 (2015).
13. L. N. Ge, H. L. Zhan, W. X. Leng, K. Zhao, and L. Z. Xiao, "Optical characterization of the principal hydrocarbon components in natural gas using terahertz spectroscopy," *Energy Fuels* **29**, 1622–1627 (2015).
14. H. L. Zhan, S. X. Wu, R. M. Bao, K. Zhao, L. Z. Xiao, L. N. Ge, and H. J. Shi, "Water adsorption dynamics into active carbon probed by terahertz spectroscopy," *RSC Adv.* **5**, 14389–14392 (2015).
15. K. Ajito and Y. Ueno, "THz chemical imaging for biological applications," *IEEE Trans. Terahertz Sci. Technol.* **1**, 293–300 (2011).
16. J. P. Landry, X. D. Zhu, and J. P. Gregg, "Label-free detection of microarrays of biomolecules by oblique-incidence reflectivity difference microscopy," *Opt. Lett.* **29**, 581–583 (2004).
17. X. D. Zhu and E. Nabighian, "In situ monitoring of ion sputtering and thermal annealing of crystalline surfaces using an oblique-incidence optical reflectance difference method," *Appl. Phys. Lett.* **73**, 2736–2738 (1998).
18. S. Liu, J. H. Zhu, L. P. He, J. Dai, H. B. Lu, L. Wu, K. J. Jin, G. Z. Yang, and H. Zhu, "Label-free, real-time detection of the dynamic processes of protein degradation using oblique-incidence reflectivity difference method," *Appl. Phys. Lett.* **104**, 163701 (2014).
19. F. Chen, H. B. Lu, Z. H. Chen, T. Zhao, and G. Z. Yang, "Optical real-time monitoring of the laser molecular-beam epitaxial growth of perovskite oxide thin films by an oblique-incidence reflectance-difference technique," *J. Opt. Soc. Am. B* **18**, 1031–1035 (2001).
20. J. Wang, H. L. Zhan, L. P. He, K. Zhao, H. B. Lü, K. J. Jin, and G. Z. Yang, "Evaluation of simulated reservoirs by using the oblique-incidence reflectivity difference technique," *Sci. China Phys. Mech. Astron.* **59**, 114221 (2016).
21. H. L. Zhan, J. Wang, K. Zhao, H. B. Lü, K. J. Jin, L. P. He, G. Z. Yang, and L. Z. Xiao, "Real-time detection of dielectric anisotropy or isotropy in unconventional oil-gas reservoir rocks supported by the oblique-incidence reflectivity difference technique," *Sci. Rep.* **6**, 39306 (2016).
22. J. Y. Wang, J. Dai, L. P. He, Y. Sun, H. B. Lu, K. J. Jin, and G. Z. Yang, "Label-free and real-time detections of the interactions of swine IgG with goat anti-swine IgG by oblique-incidence reflectivity difference technique," *J. Appl. Phys.* **112**, 064702 (2012).
23. L. P. He, S. Liu, J. Dai, L. Wu, Z. G. Liu, H. F. Wei, H. B. Lu, K. J. Jin, and G. Z. Yang, "Label-free and real-time monitor of binding and dissociation processes between protein A and swine IgG by oblique-incidence reflectivity difference method," *Chin. Phys. Lett.* **32**, 020703 (2015).
24. S. Liu, H. Y. Zhang, J. Dai, S. H. Hu, I. Pino, D. J. Eichinger, H. B. Lu, and H. Zhu, "Characterization of monoclonal antibody's binding kinetics using oblique-incidence reflectivity difference approach," *mABS* **7**, 110–119 (2015).